

Assessment of the performances of a heat exchanger in a light helicopter

Antonio Carozza*

Dipartimento di Meccanica dei Fluidi, Centro Italiano Ricerche Aerospaziali, Capua, via Maiorise 81043, Italy

(Received June 16, 2015, Revised July 27, 2015, Accepted September 7, 2015)

Abstract. This study has the aim to develop a numerical design regarding the position and the inner performances of a heat exchanger in a light helicopter. The problem was to find first of all the best position of the heat exchanger inside the engine vane in order to maximize the air flow rate capable to pass through the heat exchanger section. It is to be said that the only air contribution in the vane comes from the opening present in the roof under the main rotor. The design has been performed by means of the commercial code Fluent and using the well known grid generator ICEM CFD. Different positions are first investigated so to establish the best one. Subsequently, different areas of the opening on the roof have been considered in order to maximize even more the flow rate in the heat exchanger that was not sufficient based on the first guess of velocity, as aforementioned. At the end interesting design results are presented and discussed by contours of fields and values.

Keywords: aerodynamics; CFD simulation; heat exchanger; mass flow rate

1. Introduction

In this ESPOSA European Project framework CIRA is involved in the engine integration for the configuration PU2 and TR1, and HE1. The research activities regarding the helicopter HE1 configuration are the oil-cooler air location design and the subsequent analyses at different flow rates at the inlet. Between the different oil-cooler critical operative conditions which the airplane experiments in cruise and ground environments the most critical one is the ground flow condition and the present study has been performed just on that one.

The commercial code Fluent is used as a solver. In particular, the numerical model used in this work is the porous medium, simulated by means of a negative momentum source. The porous media are widely investigated and simulated with a number of different numerical models like Lax-Boltzman methods or finite element methods or simplified correlations methods.

In the article by (Alshrae *et al.* 2009), numerical simulations of flow and heat transfer in a serpentine heat exchanger configuration are presented to demonstrate application of porous media techniques in heat exchanger analyses. The simulations are conducted using two different approaches. In the first approach, a porous continuum homogeneous model (PCM), or macroscopic model, is applied. The solid and fluid phases are modeled as a single, homogeneous

*Corresponding author, Ph.D., Research Scientist, E-mail: a.carozza@cira.it

medium having anisotropic effective properties that are calculated separately from unit cell scale analyses and are made available to the macroscopic analysis. In the second approach, a continuum heterogeneous model (CM), or microscopic model, is employed to solve the momentum and energy equations for the fluid phase. Because the microscopic model includes computation of all the flow features, computation time is considerable. A comparison shows the advantage of using the porous-continuum model, a large savings of computation time.

Hayes *et al.* (2008) have investigated the heat transfer and fluid flow characteristics through a porous medium using numerical simulations and experiment. For the numerical simulations two models were created: a two-dimensional numerical model and a Fluent computational fluid dynamics (CFD) porous media model. The experimental investigation consisted of a flow channel with a porous medium section that was heated from below by a heat source. The results of the numerical models were compared to the experimental data in order to determine the accuracy of the models. The numerical model was then modified to better simulate a matrix heat exchanger. This numerical model then generated temperature profiles that were used to calculate the heat transfer coefficient of the matrix heat exchanger and develop a correlation between the Nusselt number and the Reynolds number.

Carozza *et al.* (2013), have presented in the occasion of AIDAA conference held at Naples in 2013 a study where the porous model has been applied to the study of isolated oil cooling ducts showing the efficiency of this study.

Even more in the article by Carozza (2015), the methodology indicated above has been deepened focusing on its CPU saving capacities and simplicity of use. The author has applied indeed the aforementioned simplified model to make a study on two kinds of very complex cooling ducts and showing how through a simple box a heat exchanger whose real internal geometry is unknown the simulation can be done without particular CFD problems taking into consideration just the problems posed by the grid generation on the external geometry.

Jahanshahi *et al.* (2010) dealt with the fluid flow simulation and thermal analysis of a two-dimensional heat recovery system using porous media. A basic high-temperature flow system is considered in which a high-temperature non-radiating gas flows through a random porous matrix. The porous medium, in addition to its convective heat exchange with the gas, may absorb, emit and scatter thermal radiation. The lattice Boltzmann method (LBM) is used to simulate fluid flow in the porous medium. The gas and solid phases are considered in non-local thermal equilibrium, and separate energy equations are applied to these phases. Convection, conduction and radiation heat transfers take place simultaneously in solid phase, but in the gas flow, heat transfer occurs by conduction and convection. For computing of radiative heat flux in the porous medium, discrete ordinates method is used to solve the radiative transfer equation. Finally the effect of various parameters on the performance of porous heat recovery system is studied.

Missirilis *et al.* (2005) did an experimental and computational study for the flow development through a heat exchanger for aero-engine applications. The heat exchanger consists of elliptic tubes in a U formation, the ends of which are attached to the collector pipe, which has a cylindrical cross section. The flow through the heat exchanger was modeled with a computational fluid dynamics approach. The heat exchanger matrices were modeled using a porous medium assumption. The pressure drop through each element of the porous medium was linked to an effective local velocity. In order to check the validity of the computational modeling, the results were compared to the measured flow parameters such as pressure and velocity distributions. The results showed that the laminar approach gave better results and this is supported by the corresponding Reynolds numbers, which indicated that the global flow field is transitional.

Missirilil *et al.* (2010) describe an effort to model the operation of a system of recuperative heat exchangers of an aero engine for real engine operating conditions. The modelling was performed with the combined use of a porous medium model and a thermo mechanical model. The porous medium model was taking into account the heat transfer and pressure loss behavior of the heat exchangers while the thermo mechanical one was used for the calculation of the wall temperature distribution of the elliptic tubes of the heat exchangers. As it is presented, the combined use of these models can provide a useful tool which can help in the prediction of the macroscopic behavior of the system of recuperative heat exchangers of the aero engine which can be used for optimization purposes and numerical studies.

Narasimhan *et al.* (2007) performed numerical methods, the effect of spatially variable permeability of porous medium tube-to-tube inter-connectors on the thermo-hydraulics of near-compact heat exchangers. Comparisons between NCHX tube bank are done using an overall enhancement ratio (ER), which was found to increase with increasing K_i of the PM inter-connectors. Treating the NCHX models as a global porous medium, useful engineering correlations are presented to predict the Nu as a function of Re and the non-dimensional global porous medium drag coefficients. Correlations predict the numerical data with $\pm 6\%$ accuracy within the range of Re tested.

Pavel and Mohamad (2004) investigate experimentally and numerically the effect of metallic porous materials, inserted in a pipe, on the rate of heat transfer. The pipe is subjected to a constant and uniform heat flux. The effects of porosity, porous material diameter and thermal conductivity as well as Reynolds number on the heat transfer rate and pressure drop are investigated. The results are compared with the clear flow case where no porous material was used. The results obtained lead to the conclusion that higher heat transfer rates can be achieved using porous inserts at the expense of a reasonable pressure drop. Also, it is shown that for an accurate simulation of heat transfer when a porous insert is employed its effective thermal conductivity should be carefully evaluated.

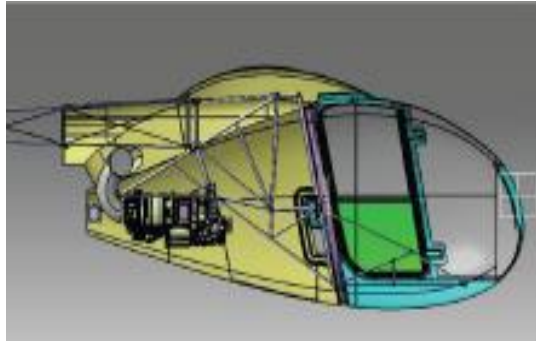
Tomimura *et al.* (2004), based on an effective energy conversion method between flowing gas enthalpy and thermal radiation, proposed a multi-layered type of gas-to-gas heat exchanger using porous media. As a result, a heat recovery section is shown to play an important role in lowering an outer wall temperature of the system and at the same time in increasing the total heat recovery rate.

The aforementioned studies are examples of how the porous medium numerical model is really efficient in simulating the performances of a heat exchanger also when the porous medium is not physically present in the heat exchanger unit.

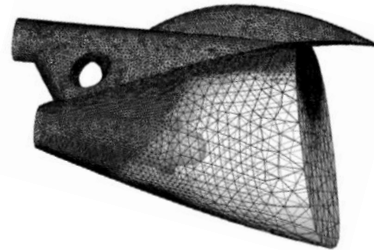
In this work, the porous media model has been applied to study the heat exchanger in a duct with the aim of investigating the efficiency of ducts to transport the right air flow rate to lower the oil temperatures and improve the engine efficiency. Oil coolers are right meshed using the grid generator ANSYS ICEM CFD and simulated by means of the commercial code FLUENT. Pressure and velocities contours together with other interesting flow field features are reported and studied in this work.

2. Governing equations and numerical methods

Numerical analysis of the flow field that takes place in each oil cooler has been carried out with Fluent in steady state turbulent flow conditions. The pressure based formulation for the ground



Reference geometry



Mesh lines overview

Fig. 1 Geometry under investigation and overview of mesh lines

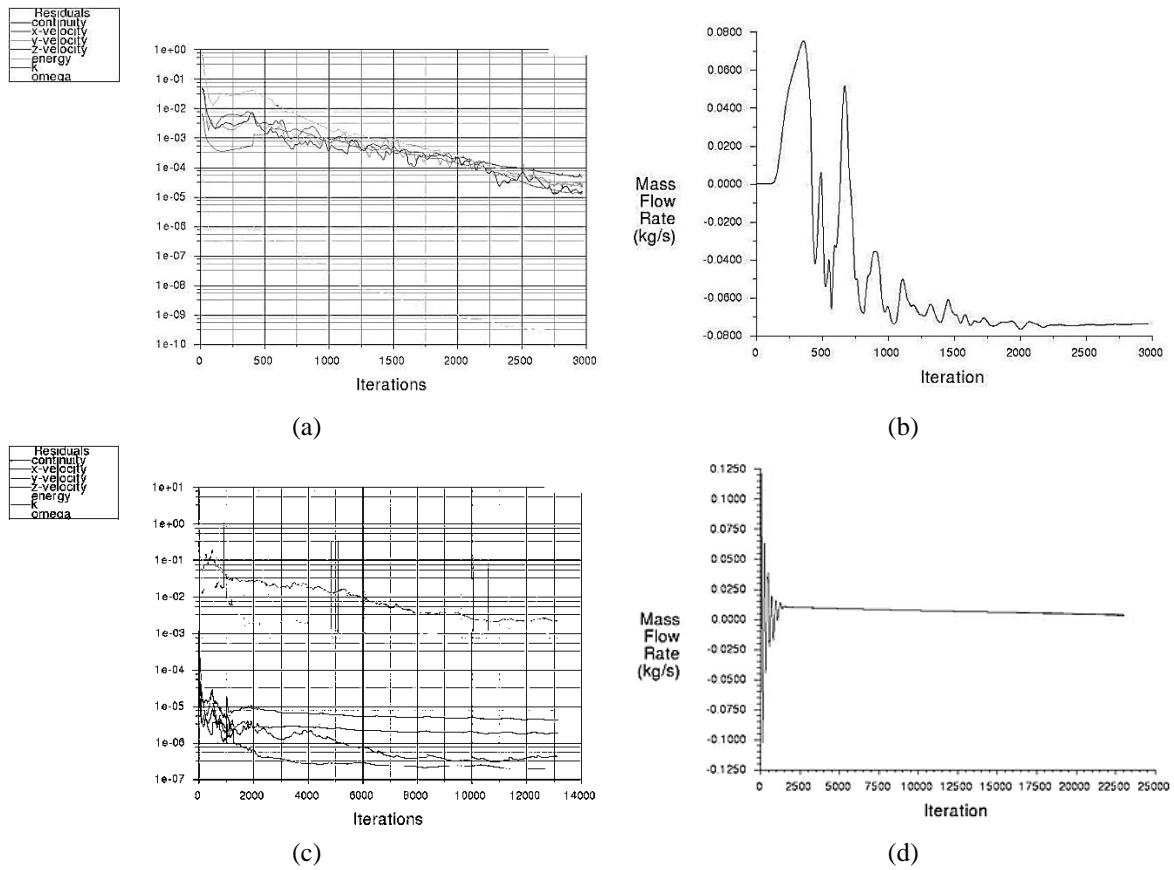


Fig. 2 Residuals and convergence examples of two computations done on ground for two different heat exchanger positions

flow condition and the implicit density based formulation for the cruise condition have been considered to solve the Reynolds averaged Navier-Stokes (RANS) equations. The first one is the classical projection method solver while the second one is a coupled scheme in which the fluid

dynamic equations are solved at the same time. An implicit formulation with a Green-Gauss Cell Based method for the gradient reconstruction is considered and the Second Order Upwind scheme for the spatial discretization is chosen for Flow, Turbulent Kinetic Energy and Specific Dissipation rate. FLUENT settings consider air as ideal-gas with a constant-averaged specific heat. Flow thermal conductivity and viscosity are set by polynomial formulation in T .

To account for turbulence, the $k-\omega$ SST model (Menter 1993) is considered with Low-Re correction enabled. The turbulent intensity (%) and turbulent viscosity ratio are set to 2 and 0.2 for both inlet and outlet (backflow) conditions.

Geometrical simplification has been done before any computation because of the complexity of the engine geometry. Numerical flow field analyses are carried out on unstructured grids, see Fig. 1, with a number of cells of about 0.4 millions of cells. The meshes are generated and built in order to reach a wall Y^+ boundary value lower than 1 to capture the velocity profile characteristics.

Fig. 2 shows some convergence and residuals histories that well clarify the criteria adopted to establish the convergence achievement.

2.1 Heat exchanger numerical model

As far as numerical model of oil cooler is concerned, it is worth to note that the heat exchange is schematized as a porous media. Therefore, the heat and pressure losses in the porous media are taken into account in the CFD computations by means of source terms in the energy and momentum flow equations, respectively. Momentum source terms in the porous media provides the air pressure drops while thermal source term determines the temperature changing of the air passing through the heat exchanger. The momentum equation reads

$$\frac{\partial}{\partial t}(\rho \vec{v}) + \nabla \cdot (\rho \vec{v} \vec{v}) = -\nabla p + \nabla \cdot \vec{\tau} + \rho \vec{g} + S \quad (1)$$

where p is the static pressure, τ is the stress tensor, g and S are the gravitational body force and external body forces, respectively. S also contains model dependent source term such as the porous media. This last term is composed of two parts: a viscous loss and an inertial loss term

$$S_i = -\left(\sum_{j=1}^3 D_{ij} \mu v_j + \sum_{j=1}^3 C_{ij} \frac{1}{2} \rho |v| v_j \right) \quad (2)$$

where S_i is the source term that appears in the i th (x, y, z) momentum equation, $|v|$ is the magnitude of the velocity. D_{ij} and C_{ij} are matrices called viscous resistance factor and inertial resistance factor. They are defined by the user for specific porous media cases. This momentum sink contributes to the pressure gradient in the porous cell, creating a pressure drop that is proportional to the fluid velocity (or velocity squared) in the cell. In the case of homogeneous porous media as for oil cooler modeling, Eq. (2) becomes

$$S_i = -\left(\frac{\mu}{\alpha} v_i + C_2 \frac{1}{2} \rho |v| v_i \right) \quad (3)$$

where α is the permeability and C_2 is the inertial resistance factor, simply specify D and C as diagonal matrices with $1/\alpha$ and C_2 on diagonals, respectively.

The heat exchanger operative data, provided by builder, allow to extrapolate the air side pressure drop versus velocity relationship and, hence, the determination of the viscous resistance

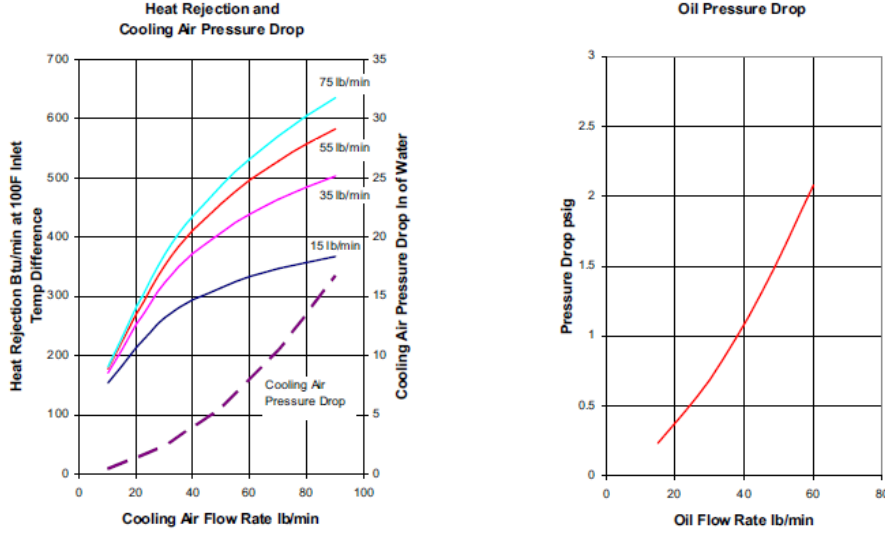


Fig. 3 Characteristics curves of the NIAGARA 2003

$(1/\alpha)$ and inertial resistance (C_2) to consider in Eq. (3). Indeed, the pressure drop versus flow velocity in the heat exchanger reads

$$\Delta p = av + bv^2 = \left(\frac{\mu}{\alpha} v + \frac{1}{2} C_2 \rho v^2 \right) \Delta n \quad (4)$$

where μ and ρ are evaluated at the operative condition altitude and Δn is the porous media thickness. Therefore

$$\frac{1}{\alpha} = \frac{a}{\mu \Delta n} \quad C_2 = \frac{2b}{\rho \Delta n} \quad (5)$$

determine the momentum source term (see Eq. (3)).

On the other hand by enabling the energy equation it is possible also to account for a thermal source term due to the porous media. Indeed, the porous media thermal generation represents the thermal power transferred to the cooling air passing through the heat exchanger.

The energy equation for the PM reads

$$\begin{aligned} & \frac{\partial}{\partial t} (\gamma \rho_f E_f + (1 - \gamma) \rho_s E_s) + \nabla \cdot (\bar{v} (\rho_f E_f + p)) \\ & = \nabla \cdot \left[k_{eff} \nabla T - \left(\sum_i h_i J_i \right) + \left(\bar{\tau} \cdot \bar{v} \right) \right] + S_f^h \end{aligned} \quad (6)$$

where E_f is the total fluid energy, E_s total solid medium energy, γ porosity of the medium, k_{eff} effective thermal conductivity of the medium and fluid enthalpy source term. The effective thermal conductivity in the porous medium, is compared by FLUENT code as the volume average of the fluid conductivity and the solid conductivity

$$\kappa_{eff} = \gamma \kappa_f + (1 - \gamma) \kappa_s \quad (7)$$

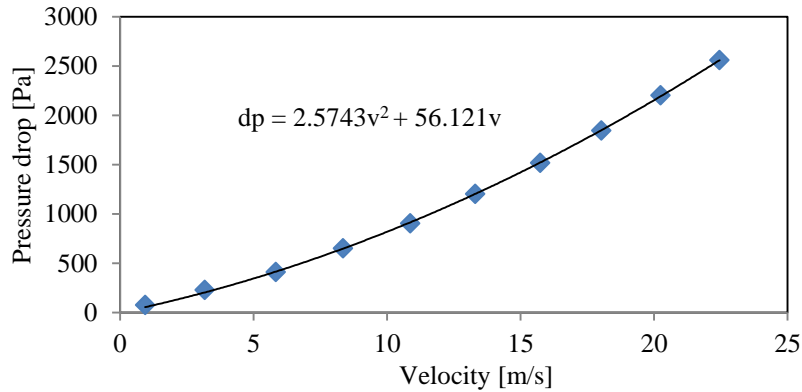


Fig. 4 Pressure drop-mean velocity curve for the heat exchanger under investigation

Table 1 Heat exchanger porous media settings

Porous medium		Thermal Power [W/m ³]
Viscous resistance 1/α [1/m ²]	Inertial resistance C ₂ [1/m]	
3.15E+07	46.1	2.23E+06

where γ is the porosity of the medium, k_f the fluid phase thermal conductivity (including the turbulent contribution) and k_s medium thermal conductivity.

The values of porous media coefficients present in Eq. (3) are computed by using the experimental data available for the heat exchanger NIAGARA 20003, see the lower curve on the left in Fig. 3.

The pressure loss-mass flow rate curve has been reported in terms of mean velocity, see Fig. 4, and a polynomial law approximating that curve has been found. At the end the coefficients of the law with the Darcy and Forcheimer coefficients are computed following the Eq. (3).

Viscous and natural resistance coefficients together with thermal generation per volume of heat exchanger considered in this research effort are provided in Table 1.

3. Discussion of results

The target of this investigation was to find the best configuration for the engine vane to enhance the heat transfer through the heat exchanger. In order to follow this objective a strategy has been adopted composed of two main points:

1. Finding the best location at a fixed inlet velocity among the suggested ones as possible
2. Finding the minimum mass flow rate at the inlet able to reach the target mass flow rate indicated by the manufacturer of 0.185 kg/s

3.1 Preliminary study on the better position of the heat exchanger inside the engine vane

A preliminary study has been conducted on the best position for the heat exchanger in order to increase the air mass flow rate passing through the exchanger. Three different positions suggested

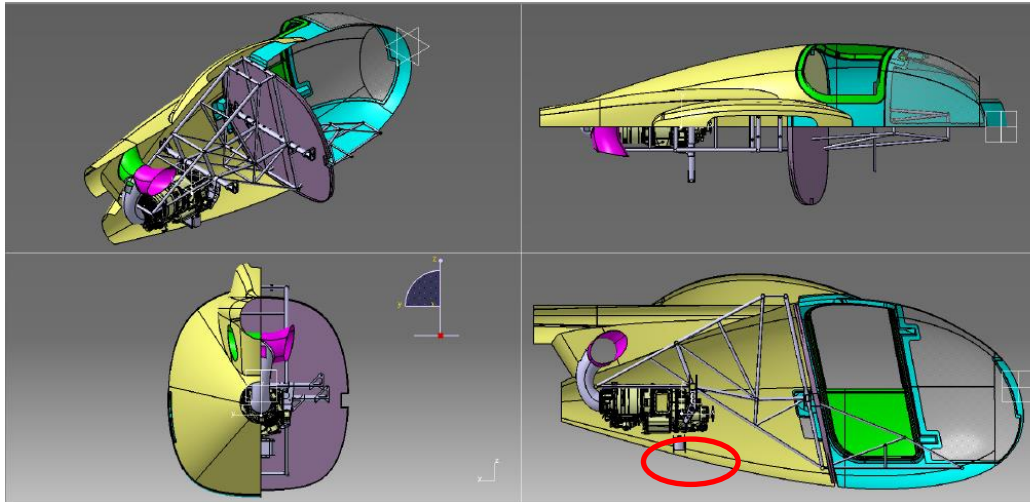
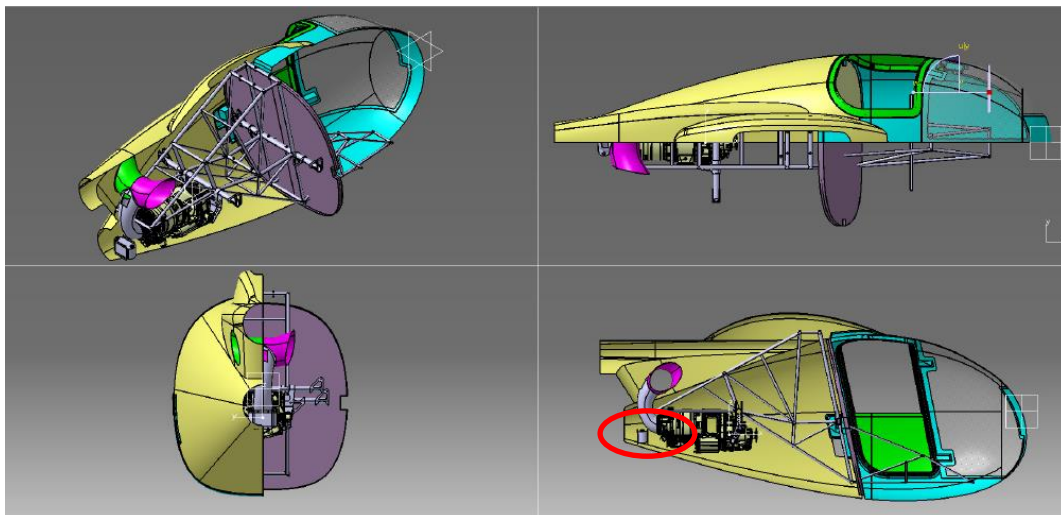
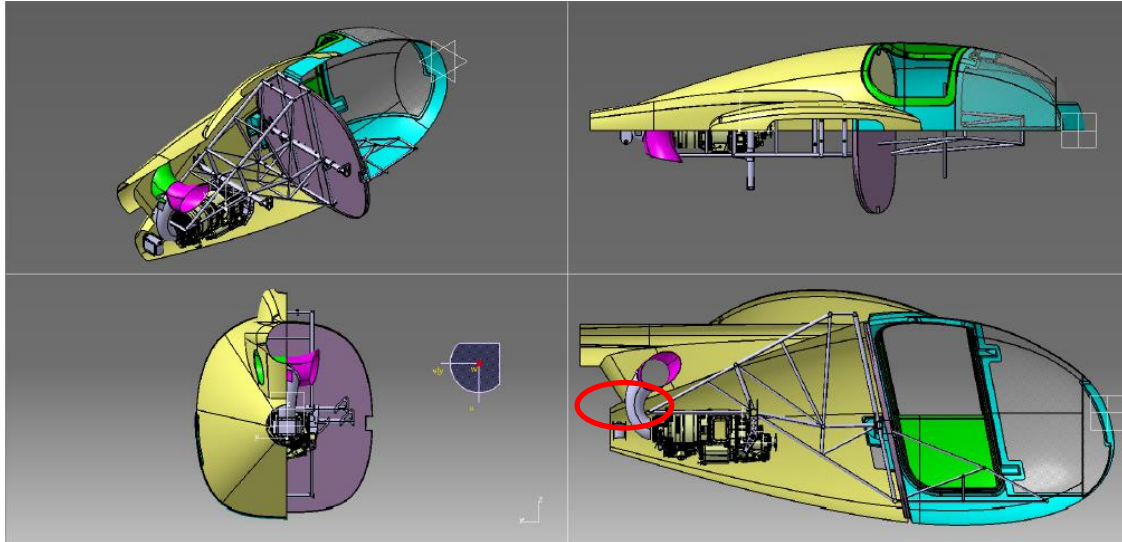
Fig. 5 1st heat exchanger positionFig. 6 2nd heat exchanger position

Table 2 Mass flow rates in the heat exchanger for its rear and more advanced position

HE position	Velocity [m/s]	Roof Mass flow rate [kg/s]	HE mass flow rate [kg/s]
1	7	1.97	0.001
2	7	1.97	0.005
3	7	1.97	0.02

by the manufacturer, see Figs. 5, 6 and 7, are considered. From Table 2, instead, it can be argued that the better position is surely the aft body one if one considers the HE mass flow rate. From a deeper analysis it seems that this location can be useful also for a simpler maintenance. It can be added that when the HE is positioned under the electronic control system, the temperature plume

Fig. 7 3rd heat exchanger position

can in some manner reach some parts of the engine and compromise the functionalities of these parts. This is another consideration that has driven to choose the lower exit as the better zone where the HE should be put.

In Fig. 8 the velocity fields inside the engine vane are shown on the symmetry plane and in the frontal section view. The velocity magnitude is greater in the case in which the HE is located near the lower exit of the case. This is likely due to a suction effect of the exit pressure on the quantity of air able to pass in the heat exchanger volume.

3.2 Parametric study on the area of inlet mass flow rate

Velocity, temperature and turbulent viscosity contours are reported below in order to illustrate the flow fields so computed. Then the mass flow rates passing through the heat exchanger section area is reported in function of the air mass flow rate coming from the roof. Figs. 9 and 10 display some flow fields regarding the flow simulations. At the end, in Fig. 11 characteristic curves are represented showing how the variation of mass flow rate through the roof opening influences the air flow rate through the heat exchanger. Fig. 9, in particular, shows what happens when a flow rate of 2.42 kg/s comes from the roof. It can be observed that the velocity values are about 6 m/s immediately upper and under the engine. However the velocity values do not overcome 18 m/s in the wakes. On the other hand the temperature reveals a plume with a size of 4 times the heat exchanger size, the same zone where a lower velocity can be detected. This is likely due to the strong presence of heat exchange in the heat exchanger and to the suction effect of the outflow boundary condition. The turbulent viscosity ratio contour instead shows how the greater instabilities are present in the region on the rear of the pilot vane. Fig. 10 is related instead to a mass flow rate on the roof of 4.83 kg/s. The velocity here achieves very high values when compared with the values of the aforementioned case. The acceleration to which the flow is subjected in the outflow zones are stronger than before when compared to the inlet values of velocity. One more time the turbulent viscosity is greater in the zone immediately close to the pilot

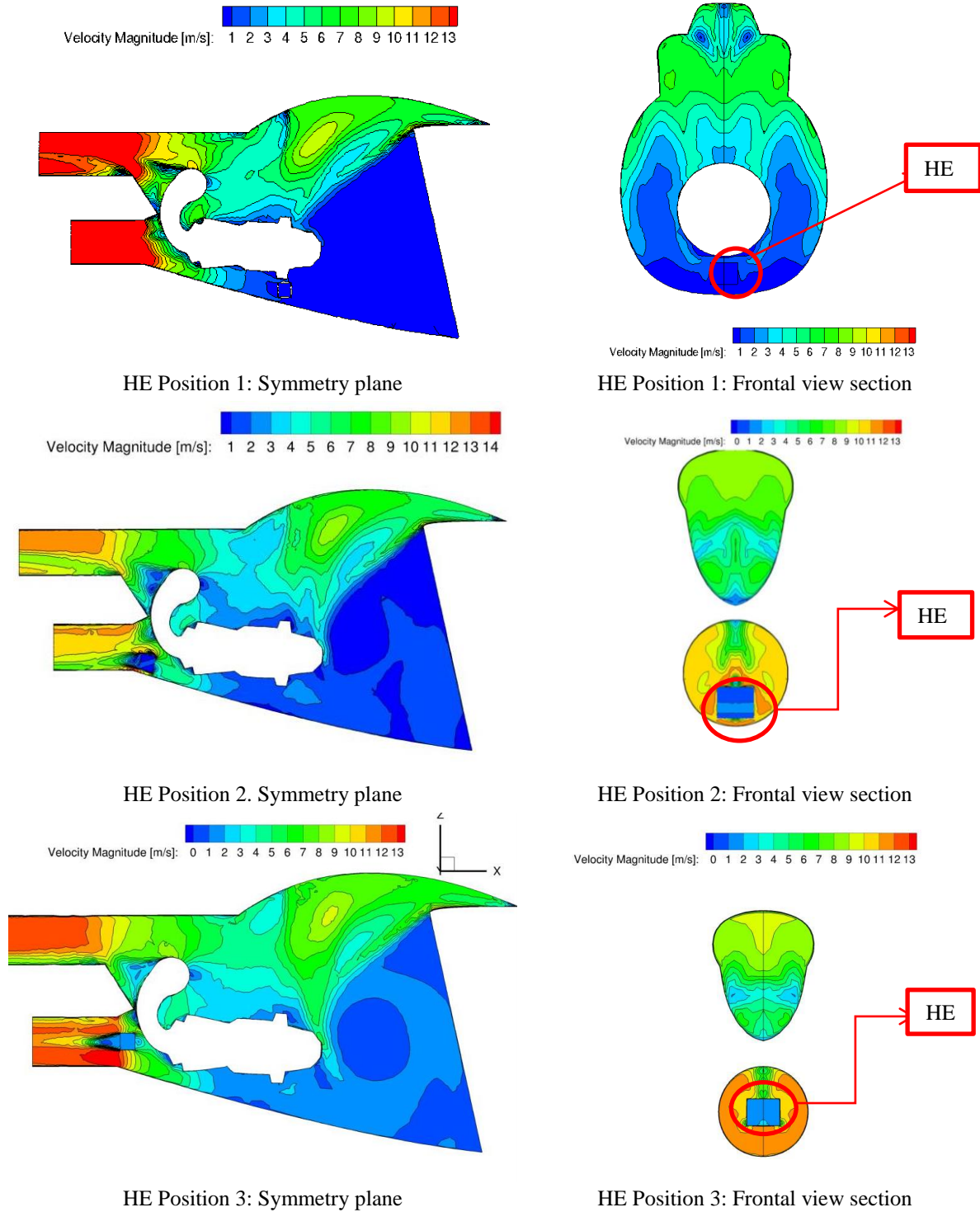


Fig. 8 Velocity contours related to the aforementioned three positions of the heat exchanger, the more advanced one and the rear one, respectively

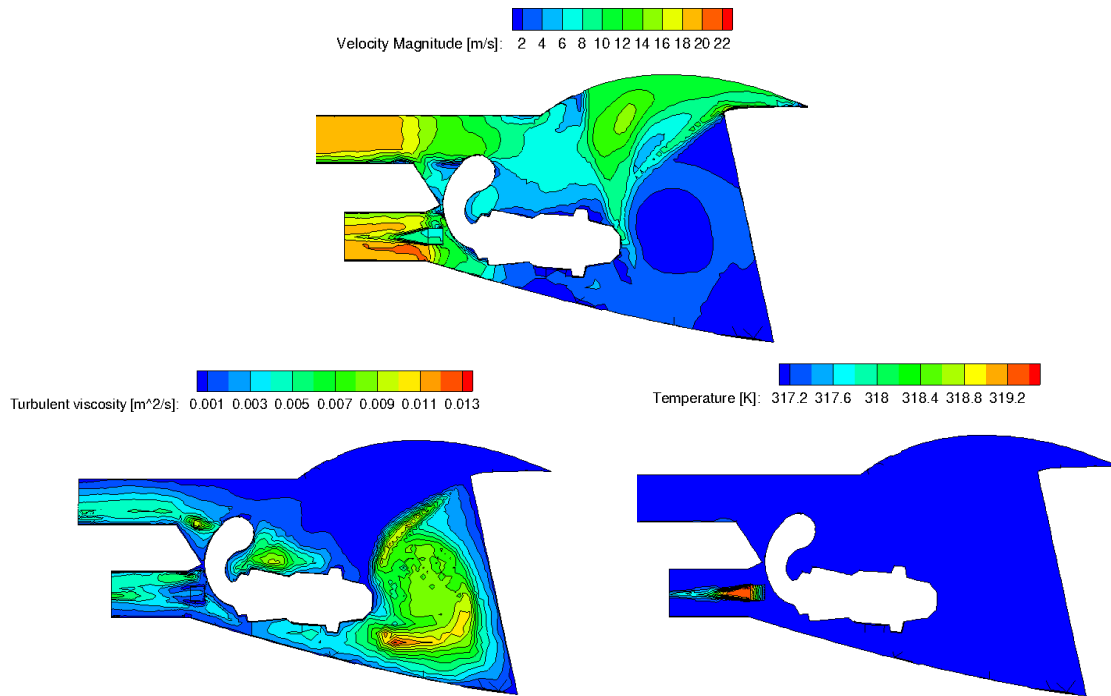


Fig. 9 Velocity, temperature and turbulent viscosity contours on the central y section for a roof mass flow rate of 2.42 kg/s (Inlet Velocity=11 m/s)

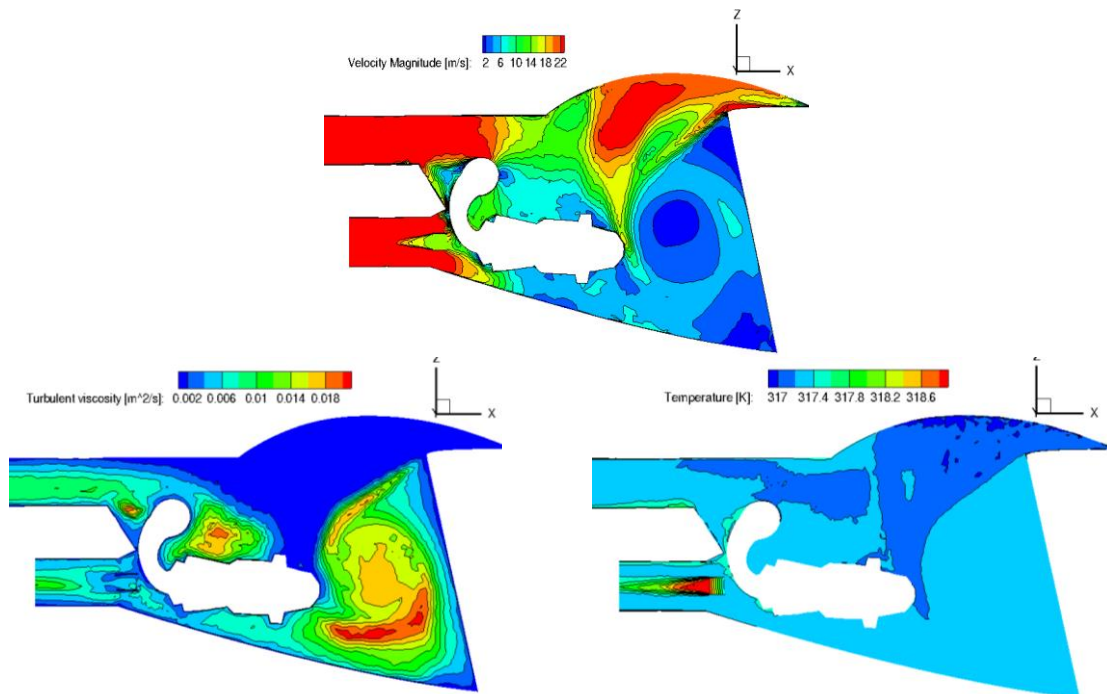


Fig. 10 Velocity, temperature and turbulent viscosity contours on the central y section for a roof mass flow rate of 4.83 kg/s (Inlet Velocity=21 m/s)

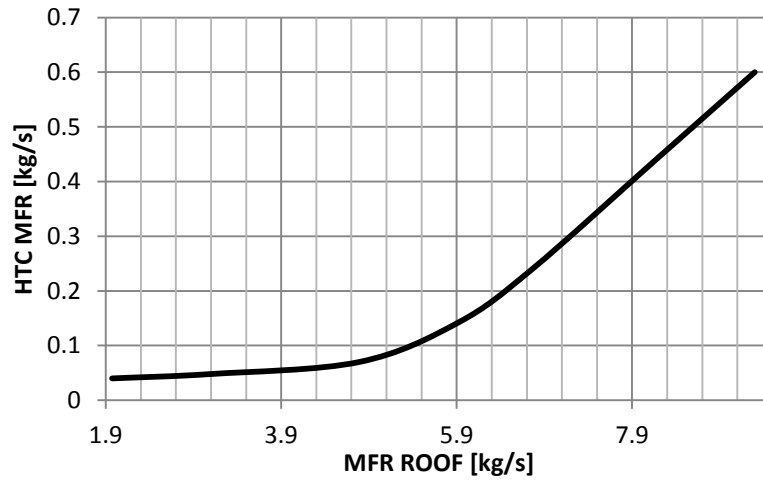


Fig. 11 Curve of heat exchanger mass flow rate [kg/s] in function of the inlet mass flow rate on the roof [kg/s]

Table 3 Mass flow rates for the two heat exchanger analyzed positions

Test case	Roof opening size [m ²]	Calculated Mass flow rate [kg/s]	Target Mass flow rate [kg/s]
1	0.21	0.02	0.185
2	0.34	0.024	0.185
3	0.52	0.035	0.185
4	0.64	0.071	0.185
5	0.74	0.12	0.185
6	0.89	0.22	0.185
7	1.01	0.305	0.185

vane. The temperature plume is more pronounced then before also because of the aforementioned stronger velocity increase in the outlet zones.

Form all of runs carried out, in some manner summarized in Table 3, it can be deduced that the best choice for the area at the inlet on the roof is about three times larger than the starting one. The Fig. 11 shows very well this behavior of the engine vane in relation with the heat exchanger air flow rate.

It is also to be said the curve represented in Fig. 11 allows to achieve the values of mass flow rates of air refreshing the engine oil directly in function of the roof opening size as reported in Table 3. It can be noticed that the aforementioned curve presents a lower inclination due to the fact that for lower roof areas the mass flow rates coming from the roof are lower and the air able to reach the heat exchanger section is very poor up to the point around the value of 3.9 kg/s beyond which the air makes a jump towards values even and even higher.

4. Conclusions

A parametric design of the heat exchanger position and mass flow rate inside a light helicopter engine vane has been done in this article. The flow condition taken into consideration is the ground idle one that is the more difficult to support thermally by an aircraft. The flow comes from above through an opening in the roof under the main rotor. The design has proceeded through two main steps. First three positions are considered as a better position for the heat exchanger; then different flow rates have been considered through the roof in order to increase the air flow rate in the HE volume. The conclusions of this design work are the following:

- The best position search requires to locate the cooling tool just near the lower exit on the rear of the helicopter case.
- The minimum flow rate coming from the roof needs to be at least 6.7 kg/s, corresponding to an area of 0.81 m², about 4 times the starting area value.

These achievements can be used also for different configurations and in other fields of the engineering practice. A future deepening of such a work could be the shape optimization of the engine vane made simpler by the HE model used herein.

References

- Alshare, A.A., Simon, T.W. and Strykowski, P.J. (2009), "Simulations of flow and heat transfer in a serpentine heat exchanger having dispersed resistance with porous-continuum and continuum models", *Int. J. Heat Mass Transf.*, **53**, 1088-1099.
- Carozza, A., Mingione, G. and Pezzella, G. (2013), "Computational flow field analyses on aeronautical oil cooling systems", *Proceedings of the 21th AIDAA Conference*, Napoli, September.
- Carozza, A. (2015), "An innovative approach for the numerical simulation of oil cooling systems", *Adv. Aircraf. Space. Sci.*, **2**(2), 169-182.
- ESPOSA Grant Agreement PART B: agreement no: 284859.
- Fluent-Commercially available CFD software package based on the Finite Volume method, A product of Fluent Inc., Centerra Resource Park, 10 Cavendish Court, Lebanon, NH, USA.
- Hayes, A.M., Khan, J.A., Shaaban, A.H. and Spearing, I.G. (2008), "The thermal modeling of a matrix heat exchanger using a porous medium and the thermal non-equilibrium model", *Int. J. Therm. Sci.*, **47**, 1306-1315.
- Jahanshahi, E., Gandjalikhan Nassab, S.A. and Jafari, S. (2010), "Thermal analysis of a 2-D heat recovery system using porous media including lattice Boltzmann simulation of fluid flow", *Int. J. Therm. Sci.*, **49**, 1031-1041.
- Menter, F.R. (1993), "Zonal two equation $k-\omega$ turbulence models for aerodynamic flows", AIAA Paper 93-2906.
- Missirilis, D., Yakinthos, K., Palikaras, A., Katheder, K. and Goulas, A. (2005), "Experimental and numerical investigation of the flow field through a heat exchanger for aero-engine applications", *Int. J. Heat Fluid Flow*, **26**, 440-458.
- Missirilis, D., Donnerhack, S., Seite, O., Albanakis, C., Sideridis, A., Yakinthos, K. and Goulas, A. (2010), "Numerical development of a heat transfer and pressure drop porosity model for a heat exchanger for aero engine applications", *Appl. Therm. Eng.*, **30**, 1341-1350.
- Narasimhan, A. and Sumuthra Raju, K.S. (2007), "Effect of variable permeability porous medium interconnectors on the thermo-hydraulics of heat exchanger modeled as porous media", *Int. J. Heat Mass Transf.*, **50**, 4052-4062.
- Pavel, B.I. and Mohamad, A.A. (2004), "An experimental and numerical study on heat transfer enhancement for gas heat exchangers fitted with porous media", *Int. J. Heat Mass Transf.*, **47**, 4939-4952.

Tomimura, T., Hamano, K., Honda, Y. and Echigo, R. (2004), "Experimental study on multi-layered type of gas-to-gas heat exchanger using porous media", *Int. J. Heat Mass Transf.*, **47**, 4615-4623.

EC